Gas-Kinetic Schemes for Fluid Simulations

Kun Xu

Mathematics Department, The Hong Kong University of Science & Technology, Clear Water Bay, Kowloon, Hong Kong

Abstract. In this paper, we are going to first present a gas-kinetic scheme based on the Bhatnagar-Gross-Krook (BGK) model for the Navier-Stokes flow simulations. Then, the relations among the BGK scheme, the central difference, Godunov, kinetic Flux Vector Splitting, and Lattice Boltzmann method will be discussed. A few comments on CFD algorithm development will also be presented.

1 Preliminaries

Based on the gas-kinetic theory, the Navier-Stokes equations can be derived from the Boltzmann equation using the Chapman-Enskog expansion. Therefore, a Navier-Stokes solver can be constructed by solving the Boltzmann equation, especially the simplified collision models [2]. In the gas-kinetic representation, all flow variables are moments of a particle distribution function. Since the gas distribution function is used to describe both equilibrium and nonequilibrium states, the inviscid and viscous fluxes are obtained simultaneously. Many kinetic schemes are based on the collisionless Boltzmann equation, $f_t + uf_x = 0$, as the governing equation to evaluate the numerical fluxes across a cell interface. The free transport mechanism implicitly sets the time step Δt as the particle collision time τ, which generates a numerical viscosity being proportional to it, i.e., $\mu_n \sim \Delta t$. Instead of solving the collisionless Boltzmann equation, a collisional BGK model is solved for the numerical fluxes in the BGK scheme, i.e., $f_t + uf_x = (g-f)/\tau$ [1]. As a result, the dissipation in the transport process is controlled by the collision time τ. This paper will present the BGK scheme for the Navier-Stokes simulations. It will be shown that the Navier-Stokes solutions can be obtained accurately in both $\tau > \Delta t$ and $\tau < \Delta t$ regions.

2 BGK Flow Solver

Following van Leer's MUSCL idea, a numerical scheme is composed of an initial reconstruction stage followed by a dynamical evolution stage. With the implementation of nonlinear limiter, the reconstructed distribution of conservative variables inside each cell becomes $\bar{w}_j(x) = w_j + L(s_+, s_-)(x - x_j)$, where w is the conservative varibales, such as the mass, momentum and energy, $s_+ = (w_{j+1} - w_j)/\Delta x$ and $s_- = (w_j - w_{j-1})/\Delta x$ are slopes, and $L(s_+, s_-)$ is the nonlinear limiter. After reconstruction, the flow distribution around a cell interface

is shown in Fig.(1). The BGK scheme is basically to present a Navier-Stokes solution based on the kinetic equation for the above initial condition.

For a 2D flow, the BGK model in the x-direction is,

$$f_t + uf_x = \frac{g-f}{\tau}, \tag{1}$$

where f is the gas distribution function and g is the equilibrium state approached by f. The particle collision time τ is related to the viscosity and heat conduction coefficients. The equilibrium state is a Maxwellian distribution,

$$g = \rho(\frac{\lambda}{\pi})^{\frac{K+2}{2}} e^{-\lambda((u-U)^2+(v-V)^2+\xi^2)},$$

where ρ is the density, U and V are the macroscopic velocities in the x and y directions, and λ is related to the gas temperature $m/2kT$. The total number of degrees of freedom K in ξ is equal to $(5-3\gamma)/(\gamma-1)+1$. In the equilibrium state, ξ^2 is equal to $\xi^2 = \xi_1^2 + \xi_2^2 + ... + \xi_K^2$. The relation between mass ρ, momentum $(m = \rho U, n = \rho V)$, and energy E densities with the distribution function f is

$$w = (\rho, m, n, E)^T = \int \psi_\alpha f d\Xi = \int \psi_\alpha g d\Xi, \qquad \alpha = 1, 2, 3, 4, \tag{2}$$

where ψ_α is the vector of moments

$$\psi_\alpha = (1, u, v, \frac{1}{2}(u^2 + v^2 + \xi^2))^T,$$

and $d\Xi = dudvd\xi$ is the volume element in the phase space with $d\xi = d\xi_1 d\xi_2 ... d\xi_K$.

The BGK scheme is based on the solution f of the BGK model at a cell interface $x_{j+1/2}$,

$$f(x_{j+1/2}, t, u, v, \xi) = \frac{1}{\tau}\int_0^t g(x', t', u, v, \xi) e^{-(t-t')/\tau} dt' + e^{-t/\tau} f_0(x_{j+1/2} - ut), \tag{3}$$

where $x' = x_{j+1/2} - u(t-t')$ is the trajectory of a particle motion and f_0 is the initial gas distribution function f at the beginning of each time step $(t = 0)$. Two unknowns g and f_0 must be specified in Eq.(3) in order to obtain the solution f. In order to simplify the notation, $x_{j+1/2} = 0$ will be used in the following text.

In a general situation, the initial gas distribution function f_0 is assumed to have the form,

$$f_0 = \begin{cases} g^l \left(1 + a^l x - \tau(a^l u + A^l)\right), & x \le 0 \\ g^r \left(1 + a^r x - \tau(a^r u + A^r)\right), & x \ge 0 \end{cases} \tag{4}$$

where a^l and a^r are coming from the spatial derivative of a Maxwellian and have a unique correspondence with the slopes of the conservative variables. The terms $-\tau(a^l u + A^l)g^l$ and $-\tau(a^r u + A^r)g^r$ account for the deviation of a gas distribution function away from a Maxwellian. The above nonequilibrium parts

are obtained from the Chapman-Enskog expansion of the BGK model, and these parts have no direct contribution to the conservative variables, i.e.,

$$\int (a^l u + A^l)\psi_\alpha g^l d\Xi = 0 \quad , \quad \int (a^r u + A^r)\psi_\alpha g^l d\Xi = 0. \tag{5}$$

The equilibrium state g around $(x = 0, t = 0)$ is assumed to have the form,

$$g = g_0 \left(1 + (1 - \mathrm{H}[x])\bar{a}^l x + \mathrm{H}[x]\bar{a}^r x + \bar{A}t\right), \tag{6}$$

where $\mathrm{H}[x]$ is the Heaviside function. Here g_0 is a local Maxwellian distribution function located at $x = 0$. Even though, g is continuous at $x = 0$, but it has different slopes at $x < 0$ and $x > 0$ regions, see Fig.(2). The dependence of $a^l, a^r, ..., \bar{A}$ on the particle velocities can be obtained from a Taylor expansion of a Maxwellian and have the following form,

$$a^l = a^l_1 + a^l_2 u + a^l_3 v + a^l_4 \frac{1}{2}(u^2 + v^2 + \xi^2) = a^l_\alpha \psi_\alpha,$$

$$...$$

$$\bar{A} = \bar{A}_1 + \bar{A}_2 u + \bar{A}_3 v + \bar{A}_4 \frac{1}{2}(u^2 + \xi^2) = \bar{A}_\alpha \psi_\alpha,$$

where $\alpha = 1, 2, 3, 4$ and all coefficients $a^l_1, a^l_2, ..., \bar{A}_4$ are local constants, which depend on temporal and spatial derivatives of the local macroscopic flow variables.

In the reconstruction stage, we have obtained the distributions $\bar{\rho}_j(x)$, $\bar{m}_j(x)$, $\bar{n}_j(x)$, and $\bar{E}_j(x)$ inside each cell $x_{j-1/2} \le x \le x_{j+1/2}$. At the cell interface $x_{j+1/2}$, the left and right macroscopic states are $\bar{w}_j(x_{j+1/2})$ and $\bar{w}_{j+1}(x_{j+1/2})$. By using the relation between the gas distribution function f and the macroscopic variables (Eq.(2)), around $x_{j+1/2}$ we get

$$\int g^l \psi_\alpha d\Xi = \bar{w}_j(x_{j+1/2}) \ ; \ \int g^l a^l \psi_\alpha d\Xi = \frac{\bar{w}_j(x_{j+1/2}) - \bar{w}_j(x_j)}{\Delta x^-} \tag{7}$$

$$\int g^r \psi_\alpha d\Xi = \bar{w}_{j+1}(x_{j+1/2}) \ ; \ \int g^r a^r \psi_\alpha d\Xi = \frac{\bar{w}_{j+1}(x_{j+1}) - \bar{w}_{j+1}(x_{j+1/2})}{\Delta x^+} \tag{8}$$

where $\Delta x^- = x_{j+1/2} - x_j$ and $\Delta x^+ = x_{j+1} - x_{j+1/2}$. The above equations uniquely determine g^l, g^r, a^l and a^r. After having a^l and a^r, A^l and A^r terms in f_0 can be found from Eq.(5).

The equilibrium state g_0 is obtained from the compatibility condition at $(x_{j+1/2}, t = 0)$,

$$\int g_0 \psi_\alpha d\Xi = w_0 = \int_{u>0} \int g^l \psi_\alpha d\Xi + \int_{u<0} \int g^r \psi_\alpha d\Xi. \tag{9}$$

Then, $\bar{a}^l$ and $\bar{a}^r$ of g in Eq.(6) can be obtained through the relation of

$$\frac{\bar{w}_{j+1}(x_{j+1}) - w_0}{\rho_0 \Delta x^+} = \int g_0 \bar{a}^l \psi_\alpha d\Xi \quad , \quad \frac{w_0 - \bar{w}_j(x_j)}{\rho_0 \Delta x^-} == \int g_0 \bar{a}^r \psi_\alpha d\Xi. \tag{10}$$

After substituting Eq.(4) and Eq.(6) into Eq.(3), the gas distribution function f at a cell interface can be expressed as

$$\begin{aligned} f(x_{j+1/2},t) = & (1-e^{-t/\tau})g_0 + \tau(t/\tau - 1 + e^{-t/\tau})\bar{A}g_0 \\ & + \left(\tau(-1+e^{-t/\tau}) + te^{-t/\tau}\right)\left(\bar{a}^l \mathrm{H}[u] + \bar{a}^r(1-\mathrm{H}[u])\right) ug_0 \\ & + e^{-t/\tau}\left((1-u(t+\tau)a^l)\mathrm{H}[u]g^l + (1-u(t+\tau)a^r)(1-\mathrm{H}[u])g^r\right) \\ & + e^{-t/\tau}\left(-\tau A^l \mathrm{H}[u]g^l - \tau A^r(1-\mathrm{H}[u])g^r\right). \end{aligned} \tag{11}$$

The only unknown term left in the above expression is $\bar{A}$. Since both f (Eq.(11)) and g (Eq.(6)) contain $\bar{A}$, the integration of the conservation constraint Eq.(2) at $x_{j+1/2}$ over the whole time step Δt determines $\bar{A}$ uniquely,

$$\int_0^{\Delta t}\int (g-f)\psi_\alpha dt d\Xi = 0.$$

Finally, the time-dependent numerical fluxes in the x-direction across the cell interface can be computed by

$$\begin{pmatrix} \mathcal{F}_\rho \\ \mathcal{F}_m \\ \mathcal{F}_n \\ \mathcal{F}_E \end{pmatrix}_{j+1/2} = \int u \begin{pmatrix} 1 \\ u \\ v \\ \frac{1}{2}(u^2+v^2+\xi^2) \end{pmatrix} f(x_{j+1/2},t,u,v,\xi)d\Xi, \tag{12}$$

where $f(x_{j+1/2},t,u,v,\xi)$ is given in Eq.(11). By integrating the above equation in a time step, we can get the total mass, momentum and energy transport.

3 Analysis

3.1 Navier-Stokes Solver

Due to the implementation of initial nonequilibrium state and the BGK gas evolution model, the BGK scheme presented in the last section gives an accurate Naver-Stokes solution in both smooth and discontinuity regions. Eq.(11) presents an explicit time-dependent gas distribution function f at the cell interface. In a resolved flow region, such as a resolved shock layer, the reconstructed conservative variables in Fig.(1) will be distributed approximately on a straight line. In such a case, the gas distribution function f at a cell interface becomes

$$f = g_0(1-\tau(u\bar{a}+\bar{A}) + t\bar{A}), \tag{13}$$

where $-\tau(u\bar{a}+\bar{A})g_0$ is exactly the nonequilibrium state in the Chapman-Enskog expansion of the BGK model [23], and $g_0\bar{A}t$ is the temporal evolution part of the gas distribution function. The above equation (13) is actually the equation we used for the low Mach number viscous flow calculations [18]. Eq.(13) is basically a kinetic Lax-Wendroff type scheme for the Navier-Stokes equations. Therefore, in the smooth flow region the BGK method goes to a 2nd-order central difference scheme.

3.2 Collision time

In a well resolved dissipative region, such as the cell size Δx is smaller than the dissipative length scale determined by the physical viscosity, the collision time τ in the BGK scheme can be determined by the relation $\tau = \mu/p$, where μ is the dynamical viscosity coefficient and p is the pressure. Theoretically, any dissipative structure, such as the shock thickness, is determined by the physical viscosity, and the structure should be independent of the cell size. However, even though the Navier-Stokes equations are solved accurately by the BGK method, if the cell size is not fine enough to resolve the wave structure, the physical wave structure has to be replaced by a numerical one, such as the physical shock thickness being replaced by the numerical cell size. In such a situation, we cannot solve the Navier-Stokes equations with the original physical viscosity. The effective viscosity should be a combination of the physical and numerical ones. Different from many upwinding schemes, the BGK method cannot simply take the apology to say that the implicit numerical viscosity is included in the under-resolved flow region. Since the BGK method is so accurate in solving the Navier-Stokes equations even in the under-resolved discontinuity region, the required additional numerical viscosity has to be explicitly included. Because the jump in the flow variables at a cell interface, see Fig.(1), represents the under resolveness and it appears automatically in high gradient flow region, the collision time τ used in all simulations will take the jump into account,

$$\tau = \frac{\mu}{p} + \frac{|p^l - p^r|}{|p^l + p^r|}\Delta t, \tag{14}$$

where Δt is the CFL time step and the second term provides the numerical viscosity, which is a function of the pressure jump at the cell interface in the reconstructed initial data. The obvious advantage of the BGK method is that it solves a viscous equation with an explicit dissipative coefficient, which avoids the ambiguity of implicit dissipation in many upwinding schemes. Even though the shock jump can be captured nicely in the Godunov type schemes, but the dissipation to construct such a wide shock transition is mainly coming from numerics. It does not guarantee that the same numerical dissipation will not poison the physical viscous solution, or the dissipation will appear when necessary in multidimensional case.

Even the Navier-Stokes equations with an adaptive local viscous coefficient can be solved by the Godunov-type method, there are still difference between it and the BGK method. The BGK scheme gives a solution directly under the general initial condition (Fig.(1)), it is difficult to design an unsplitting Godunov method for the Navier-Stokes equations from the same initial condition. Even for the same mass, momentum, and energy distributions, see Fig.(1) again, the kinetic scheme uses a non-equilibrium state f_0 to describe it. The macroscopic description could only see an equilibrium state.

3.3 KFVS Limit

The BGK scheme is valid for the Navier-Stokes solution in both $\tau < \Delta t$ and $\tau > \Delta t$ region. In the limit of $\tau >> \Delta t$, the solution of the gas distribution function f in Eq.(11) reduces to

$$f = (1 - \tau(ua^l + A^l))\mathrm{H}[u]g^l + (1 - \tau(ua^r + A^r))(1 - \mathrm{H}[u])g^r. \qquad (15)$$

This distribution is similar to the one used by Chou and Baganoff in their Kinetic Flux Vector Splitting (KFVS) Navier-Stokes (NS) solver [6]. In their approach, a direct implementation of the Chapman-Enskog distribution of the Boltzmann equation is used to split the flux. From the BGK scheme, we can clearly understand the limitation of the Chou-Baganoff's Kinetic KFVS NS method. Because Eq.(15) is the limiting case of Eq.(11) when $\tau >> \Delta t$, Eq.(15) is only valid for the Navier-Stokes solution under such a limiting condition. In other words, KFVS NS scheme approaches the Navier-Stokes solution accurately only in the case $\mu/p >> \Delta t$.

For the Euler solutions, Eq.(15) can be further simplified,

$$f = \mathrm{H}[u]g^l + (1 - \mathrm{H}[u])g^r, \qquad (16)$$

where the nonequilibrium state is totally removed. This is precisely the KFVS scheme for the compressible Euler equations [15,11]. A earlier version of the above scheme is the beam scheme, where instead of Maxwellians the equilibrium states g^l and g^r are replaced by three Delta functions or particles [16]. As analyzed recently [19], the Steger-Warming method can be represented as a "beam scheme". Because of their slight difference in the particle representation, the Steger-Warming method is less robust than the beam scheme due to the lack of internal energy in its second "particle". Physically, the KFVS, beam, Steger-Warming and many other FVS schemes are equivalent. Therefore, it is easy to understand the poor performance of FVS schemes in the viscous boundary layer calculations [17,20,21], where the condition $\mu/p >> \Delta t$ is not satisfied once there are only a few grid points in the boundary layer.

Lattice Boltzmann method is very fortunate in this aspect. It does present an accurate NS solution in the incompressible limit [4]. The reason for this is that with a symmetric lattice, the free particle transport from one node to another node (no averaging) could generate anti-diffusive term which is consistent with the incompressible Navier-Stokes equations and the viscous coefficient is proportional to $-\frac{1}{2}\Delta t$. Therefore, the numerical dissipative term can be absorbed in the physical one [10]. As a result, the final viscosity coefficient in the Lattice BGK model is proportional to $(\tau - \Delta t/2)$, where $\Delta t = 1$ is used there. There is no a precise analogue between the KFVS scheme and the Lattice BGK method. Due to cell averaging process and the non-isotropic mesh, such as the lack of diagonal transport, the KFVS scheme has a much more complicated dissipative mechanism. But, the numerical viscosity coefficient ν_n can be still estimated using a simple shear flow model, which shows $\nu_n \sim \Delta t/2$. We believe that the development of a multidimensional scheme will depend not only on the *wave*

modeling, but also on the *mesh construction*. It depends closely on wether a numerical mesh could preserve the isotropic property of the fluid equations. CFD community usually has less experience in this aspect. There is something we can learn from the Lattice Boltzmann method, where the symmetry, invariants, etc., are the main concerns in their algorithm developments. Recently, it has been realized by the CE/SE method that a triangular mesh is important to preserve the conservation in space and time and avoid the reconstruction or interpolation [5]. In some sense, a triangular mesh has more symmetry and isotropic properties than a rectangular one.

3.4 Slip Boundary Condition

Another important observation of the kinetic scheme is that it can introduce slip condition in the Navier-Stokes formulation naturally through the use of appropriate flux boundary condition. The basic formulation of kinetic slip boundary is based on the fact that with the introduction of gas distribution function, we can explicitly evaluate the amount of particles hitting the boundary, then according to the accommodation coefficients for the momentum and energy, or the temperature at the wall, we can re-emit the same amount of particles with a pre-described distribution function. As a result, the appearance of slip at the boundary is obtained naturally, and this step is consistent with the DSMC type boundary condition in the near continuum regime due to their common kinetic considerations. Therefore, the kinetic method is the one which can cover the whole spectrum from the Euler and Navier-Stokes to near continuum region, where a slip boundary can be used to match it to the DSMC method.

3.5 Prandtl Number Fix

It is well known that the BGK model corresponds to a unit Prandtl number. In order to change the above Prandtl number to any realistic value, many attempts have been proposed, such as the BGK-Ellipsoidal-Statistical (BGK-ES) collision operator [9]. The BGK model itself can always make one coefficient correct, the viscosity or heat conduction. From the BGK method, we have obtained explicitly the time dependent gas distribution function at the cell interface Eq.(11). Therefore, the heat flux can be precisely evaluated,

$$q = \frac{1}{2}\int (u-U)\left((u-U)^2+(v-V)^2+\xi^2\right) f d\Xi, \tag{17}$$

where the average velocities U and V are

$$U = \int u f d\Xi \Big/ \int f d\Xi \quad , \quad V = \int v f d\Xi \Big/ \int f d\Xi.$$

Then, the easiest way to fix the Prandtl number for the BGK scheme is to modify the energy flux by subtracting the above heat flux (17) and adding another amount with a correct Prandtl number,

$$F_E^{new} = F_E + (\frac{1}{\mathrm{Pr}} - 1)q, \tag{18}$$

where F_E is the energy flux in the original BGK scheme. A simple method to evaluate q is proposed in [3]. We believe that the above fix can be equally applied to the BGK Discrete Velocity Model (DVM), where the discrete distribution function f is known [12].

The Prandtl number fix (18) is a post-processing correction, which is basically a numerical fix. But, we believe that to the Navier-Stokes order, the above fix will work perfectly. Actually, the BGK-ES model is a numerical fix on the dynamical level. But, dynamically keeping an anisotropic Gaussian for the equilibrium distribution function seems no any physical basis. The real physical weakness of the BGK model is that the collision time is independent of particle velocity, this fact is different from the phenomena with an anisotropic temperature distribution, where the temperature is directionly dependent.

3.6 Artificial viscosity – Godunov – BGK method

In the CFD algorithm development, the two classical pioneering papers for the shock capturing schemes are by von Neumann and Richtmyer [22] and by Godunov [7]. Since any physical solution has to be described in the discretized space and time, the limitation of cell size and time step has to be considered. von Neumann and Richtmyer realized that the numerical shock thickness needs to be compatible with the cell size. So, the central idea in [22] is that a viscous governing equation with an enhanced viscosity coefficient has to be solved numerically.

The success in Godunov method is that he introduced a discontinuity in the flow representation. For the under resolved flow simulation, due to the large cell size, a discontinuity will naturally appear in the initial data. The implementation of a discontinuity is much more important than the introduction of the Riemann solver. The cell interface discontinuity gives a more realistic representation about the physical solution and the numerical dissipation involved in the discontinuity can hardly be recovered by a delicate viscosity coefficient. But, as we go to a second order scheme and include the non-linear limited slopes, the relability of the numerical dissipation inside the initial data for the capturing discontinuity solution becomes questionable. From our experience, we believe that if a *Generalized Riemann Solver* is used to solve the *Euler equations* with the inclusion of initial slopes in the gas evolution stage, see Fig.(1), a 2nd-order (in both space and time) scheme cannot properly capture the numerical shock waves. Even with the discontinuity at a cell interface, additional numerical dissipation is still needed.

The methodology of the BGK scheme is in somehow to combine the two important issues rised in the above two methods, 1. a viscous governing equation with an enhanced viscosity coefficient (14) is solved. 2. Account the discontinuity and slopes of the initial data in the gas evolution stage. Both factors are important for the development of a robust scheme for the fluid simulation. In the smooth region, the additional numerical viscosity and the discontinuity at the cell interface disappear. The BGK scheme goes back to the traditional Lax-Wendroff type central schemes for NS equations.

4 Numerical Experiments

Case(1) Couette Flow with a Temperature Gradient Couette flow with a temperature gradient provides a good test for the BGK scheme to describe the viscous heat conducting flow. With the bottom wall fixed, the top boundary is moving at a speed U. The temperatures at the bottom and top are fixed with values T_0 and T_1. The analytic steady state temperature distribution is

$$\frac{T - T_0}{T_1 - T_0} = \frac{y}{H} + \frac{\mathrm{PrEc}}{2}\frac{y}{H}(1 - \frac{y}{H}), \tag{19}$$

where H is the height of the channel, Pr is the Prandtl number, Ec is the Eckert number $\mathrm{Ec} = U^2/C_p(T_1 - T_0)$, and C_p is the specific heat ratio at constant pressure. The BGK solutions with 20 grid points are shown in Fig.(3). The Prandtl number fix does modify the heat conduction term correctly.

Case(2) Navier-Stokes Shock Structure This case is to show the performance of the BGK scheme from the shock capturing to shock structure calculation. Initially, a stationary shock with Mach number $\mathrm{M} = 1.5$ is located at $x = 0$. The physical viscosity coefficient for the BGK scheme takes a value $\nu = 0.00025$, which corresponds to a shock thickness, $l_s \sim 1/300$. The density distributions with different cell sizes are shown in Fig.(4).

Case(3) Mach 3 Step Problem The computation is carried out on a uniform mesh with 120×40 cells, and the cell size used is $\Delta x = \Delta y = 1/40$. In order to test the viscous effect on the flow structure, we have used different Reynolds number $\mathrm{Re} = UL/\nu = 10^5$ and 50. The adiabatic slip Euler condition is imposed at the boundaries in order to avoid the formation of viscous boundary layer. The density and pressure distributions at different Reynolds number are presented in Fig.(5) and (6). The shock structure in (6) is well resolved.

Case(4) Laminar Boundary Layer Case A laminar boundary layer with Mach number $M = 0.15$ and $\mathrm{Re} = 10^5$ is tested over a flat plate. A rectangular mesh with 120×30 grid points clustering above the flat plate is used. The U and V velocity distributions at two locations are plotted in Fig.(7). Due to the high Reynolds number in this case, the physical collision time τ determined by the viscosity coefficient is much smaller than the time step Δt, i.e., $\tau << \Delta t$. There will have difficulties for the KFVS NS method to calculate this case.

Case(5) Shock Boundary Layer Interaction This test is about the interaction of an oblique shock at an angle 32.6^0 with a boundary layer. The Mach number of the shock wave is $M = 2.0$ and the Reynolds number for the upstream flow is $\mathrm{Re} = 2.96 \times 10^5$. The dynamical viscosity μ used here is the Sutherland's law, and the Prandtl number is equal to 0.72. A mesh clustering around the flat plate with 110×60 grid points are constructed. The skin friction and pressure distributions at the surface of the plate is shown in Fig.(8).

Case(6) A M_s=1.22 shock wave in air hits a Helium cylindrical bubble The BGK scheme has been recently extended to two component flow simulation. In the multicomponent case, each component has its individual BGK model and the momentum and energy coupling are achieved through the collision terms. The application to the shock-bubble interaction is shown in Fig.(9).

5 Conclusion

A gas-kinetic BGK scheme for the fluid simulations is presented in this paper. Due to the implemetation of non-equilibrium state at the beginning of each time step and the BGK gas evolution model, the BGK method could give accurate NS solution in both smooth and discontinuity regions. The KFVS method and the Lax-Wendroff type schemes are the limiting cases of the current kinetic BGK method. The comprehensive numerical results presented in this paper and the physical and numerical analysis about the scheme indicate the level of maturity achieved by the gas-kinetic method.

References

1. P.L. Bhatnagar, E.P. Gross, and M. Krook, Phys. Rev., **94** (1954), pp. 511.
2. G.A. Bird, Orford Science Publications (1994).
3. D. Chae, C. Kim, and O. Rho, J. Comput. phys., **158** (2000), pp. 1-27.
4. S. Chen and G. Doolen, Ann. Rev. Fluid Mech., **30** (1998), pp. 329-364.
5. S.C.Chang, et. al., CFD Review 1998, M. Hafez and K. Oshima eds..
6. S.Y. Chou and D. Baganoff, J. Comput. Phys., **130** (1997), pp. 217-230.
7. S.K. Godunov, Math. Sbornik, **47** (1959), pp. 271.
8. R.J. Hakkinen, et. al., NASA Memo. 2-18-59W (1959).
9. L.H. Holway, Rarefied Gas Dynamics, Vol. 1 (1966), pp. 193-215.
10. M. Junk and S.V.R. Rao, J. Comput. Phys., **155** (1999), pp. 178-198.
11. J.C. Mandal and S.M. Deshpande, Computers & Fluids, **23** (1994), pp. 447.
12. L. Mieussens, to appear in J. Comput. Phys. (2000).
13. G.N. Patterson, *Molecular Flow of Gases*, Wiley, New York (1956).
14. K.H. Prendergast and K. Xu, J. Comput. Phys., **109** (1993), pp. 53.
15. D.I Pullin, J. Comput. Phys., **34** (1980), pp. 231-244.
16. R.H. Sanders and K.H. Prendergast, Astrophy. Journal, **188** (1974).
17. J. L. Steger and R. F. Warming, J. Comput. Phys., **40** (1981), pp. 263-293.
18. M.D. Su, K. Xu, M. Ghidaoui, J. Comput. Phys., **150** (1999), pp. 17-39.
19. H.Z. Tang and K. Xu, accepted by ZAMP (2000).
20. B. van. Leer, ICASE report, NO.82-30 (1982).
21. B. van. Leer, J.L. Thomas, P.L. Roe, R.W. Newsome, AIAA 87-1104.
22. J. von Neumann and R.D. Richtmyer, J. Appl. Phys., **21** (1950), pp. 232-237.
23. K. Xu, VKI Lecture Series 1998-03 for Computational Fluid Dynamics.
24. K. Xu, L. Martinelli, and A. Jameson, J. Comput. Phys., **120** (1995), pp. 48.

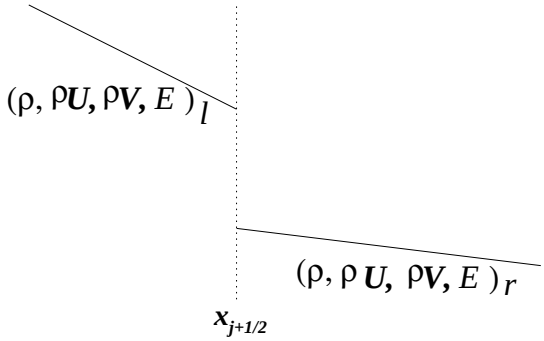

Fig. 1. Reconstructed initial conservative variables around a cell interface, from which the nonequilibrium state f_0 is constructed.

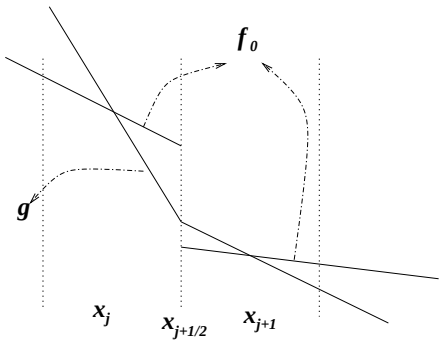

Fig. 2. The spatial distribution of the initial state f_0 and the equilibrium state g at $t = 0$.

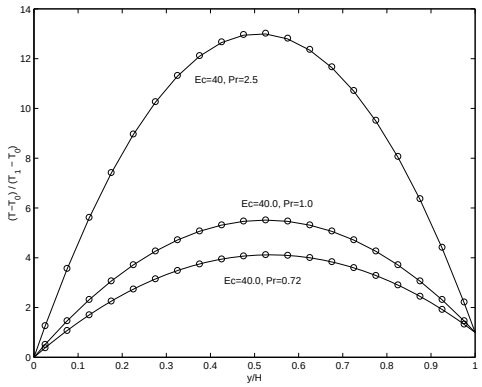

Fig. 3. Temperature ratio $(T - T_0)/(T_1 - T_0)$ in Couette flow. The solid line is the analytic solution and the circles are the numerical ones from the BGK scheme.

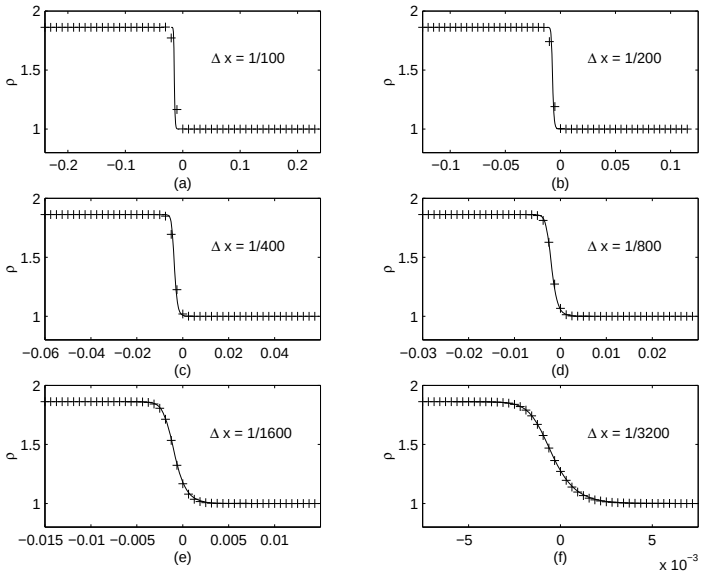

Fig. 4. Density distribution of a stationary shock wave with $M = 1.5$. The numerical solution (+ sign) is obtained from the BGK scheme with different cell sizes. The solid lines are the exact Navier-Stokes solution.

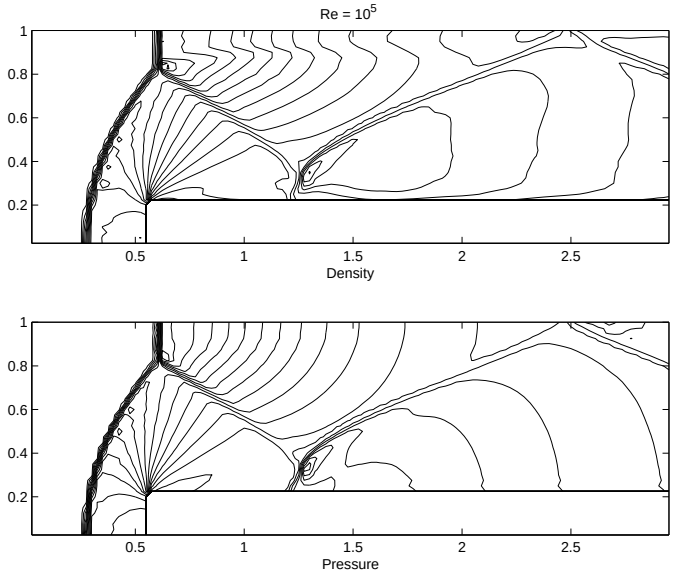

Fig. 5. Density and pressure contours in Mach 3 step problem on a mesh with 120×40 grid points. The Reynolds number used in this case is Re=10^5 w.r.t. the upstream velocity $U = 3.0$ and the channel height $L = 1.0$.

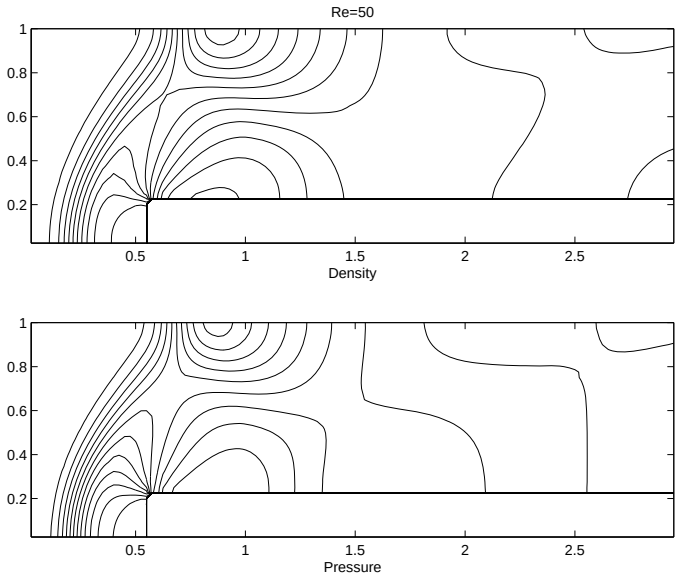

Fig. 6. Density and pressure contours. The Reynolds number is Re=50.

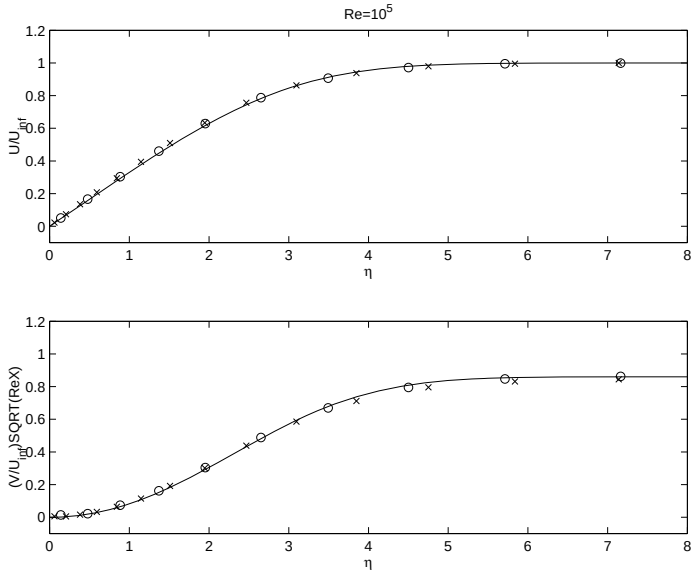

Fig. 7. U (upper) and V (lower) velocity distributions along the vertical lines at two different location of the boundary. The solid lines are the exact Blasius solutions.

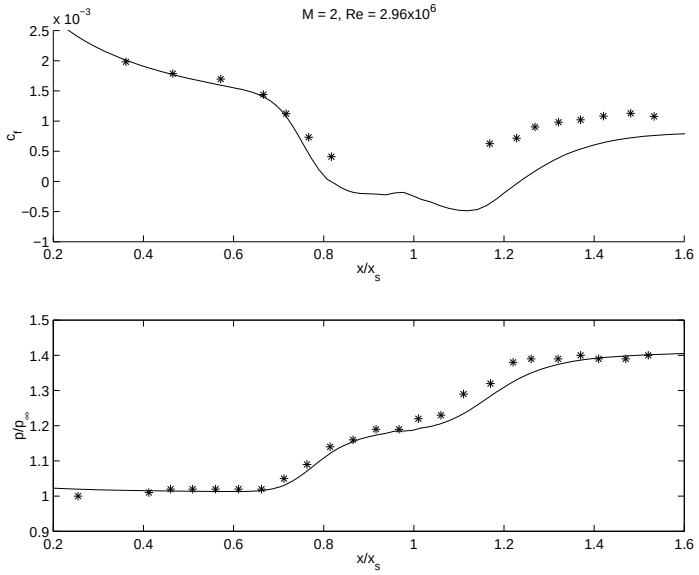

Fig. 8. Shock-boundary interaction case. (upper): skin friction, (lower): pressure distribution, along the flat plate. The $*$ is the experimental data [8]. Solid line: numerical solution. The computation is done on a mesh with 110×60 grid points.

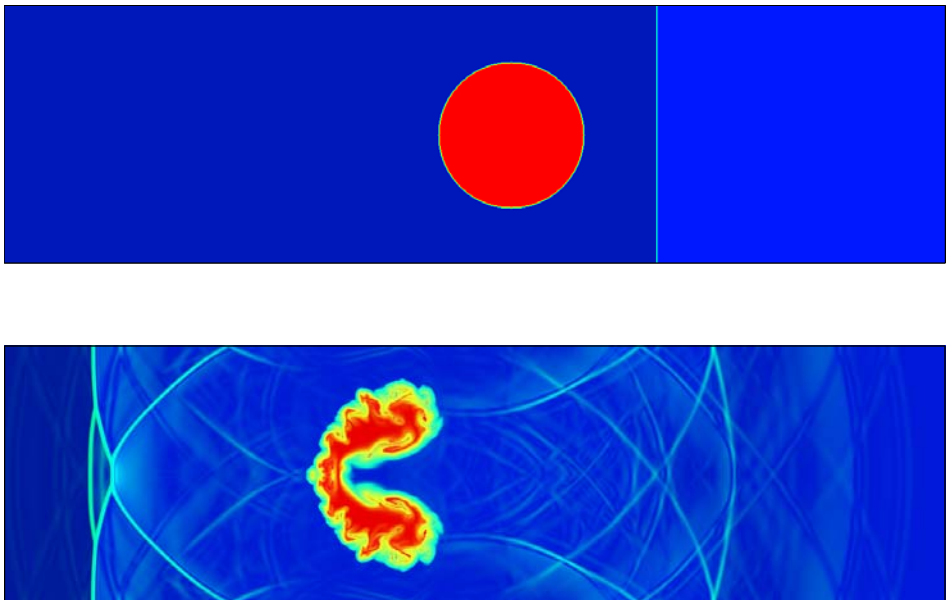

Fig. 9. Numerical Schlieren images of the interaction between a M_s=1.22 shock wave in the air and a Helium cylindrical bubble. The shock is moving from right to left. The second image describe the fields of the density gradient distribution after collision.